HHS Public Access

Author manuscript

Mol Carcinog. Author manuscript; available in PMC 2016 March 22.

Asiatic acid induces endoplasmic reticulum stress and apoptotic death in glioblastoma multiforme cells both *in vitro* and *in vivo*

Chandagirikoppal V. Kavitha[1], **Anil K. Jain**[1], **Chapla Agarwal**[1,2], **Angela Pierce**[3], **Amy Keating**[3], **Kendra M. Huber**[2,4], **Natalie J. Serkova**[2,4], **Michael F. Wempe**[1,2], **Rajesh Agarwal**[1,2], and **Gagan Deep**[1,2,*]

[1]Department of Pharmaceutical Sciences, Skaggs School of Pharmacy and Pharmaceutical Sciences, Colorado

[2]University of Colorado Cancer Center, Colorado

[3]University of Colorado School of Medicine, Department of Pediatrics, Colorado

[4]Department of Anesthesiology, University of Colorado Denver Aurora, Colorado

Abstract

Glioblastoma multiforme (GBM) is an untreatable malignancy. Existing therapeutic options are insufficient, and adversely affect functional and non-cancerous cells in the brain impairing different functions of the body. Therefore, there is an urgent need for additional preventive and therapeutic non-toxic drugs against GBM. Asiatic acid (AsA; 2,3,23-trihydroxy-12-ursen-28-oic acid, $C_{30}H_{48}O_5$) is a natural small molecule widely used to treat various neurological disorders, and the present research investigates AsA's efficacy against GBM both *in vitro* and *in vivo*. Results showed that AsA treatment (10–100 μM) decreased the human GBM cell (LN18, U87MG, and U118MG) viability, with better efficacy than temozolomide at equimolar doses. Orally administered AsA (30 mg/kg/day) strongly decreased tumor volume in mice when administered immediately after ectopic U87MG xenograft implantation (54% decrease, $p \leq 0.05$) or in mice with established xenografts (48% decrease, $p \leq 0.05$) without any apparent toxicity. Importantly, AsA feeding (30 mg/kg/twice a day) also decreased the orthotopic U87MG xenografts growth in nude mice as measured by magnetic resonance imaging. Using LC/MS-MS methods, AsA was detected in mice plasma and brain tissue, confirming that AsA crosses blood-brain barrier. Mechanistic studies showed that AsA induces apoptotic death by modulating the protein expression of several apoptosis regulators (caspases, Bcl2 family members, and survivin) in GBM cells. Furthermore, AsA induced ER stress (increased GRP78 and Calpain, and decreased Calnexin and IRE1α expression), enhanced free intra-cellular calcium, and damaged cellular organization in GBM cells. These experimental results demonstrate that AsA is effective against GBM, and advocate further pre-clinical and clinical evaluations of AsA against GBM.

Keywords

Glioblastoma multiforme; Asiatic acid; ER stress; Apoptosis; Calcium

[*]Corresponding Author: Gagan Deep, 12850 E. Montview Blvd, C238, Aurora, CO 80045. Phone: (303) 724-5553, Fax: (303) 724-7266, Gagan.deep@ucdenver.edu.

INTRODUCTION

The American Cancer Society has reported that many malignant glioma patients (~77%) die within twelve months after being diagnosed; hence, malignant glioma has a high mortality rate [1,2]. Despite several treatment options which include surgical de-bulking, radio- and chemo-therapy, glioma patient prognosis is very poor. Many therapeutic approaches also adversely alter non-cancerous brain cells and thereby distort various normal body functions. Consequently, alternative strategies to improve glioma patient survival are needed. Preventing or inhibiting glioma growth and progression using non-toxic and effective natural small molecules is an attractive strategy. The current research investigates asiatic acid (AsA; 2,3,23-trihydroxy-12-ursen-28-oic acid, $C_{30}H_{48}O_5$), a pentacyclic triterpene found in *Centella asiatica* (Family, Umbelliferae), and its anti-cancer effectiveness. In traditional medicine, *Centella asiatica* extract has been extensively used to treat nervous disorders [3–8]. AsA's neuroprotective efficacy has been shown against glutamate- or beta-amyloid-induced neurotoxicity, cognitive deficits, and focal cerebral ischemia [9–11]. AsA has also been reported to induce apoptotic death in several human cancer cell lines including colon, breast, glioma, melanoma, prostate, and hepatic [12–19]. Park *et al* have reported that AsA inhibits 7,12-dimethylbenz[a]anthracene and 12-O-tetradecanoylphorbol 13-acetate-induced skin tumor formation via targeting NO and COX2 [20]. Recently, we reported that AsA inhibits pro-angiogenic effects of VEGF and glioma cells on endothelial cells [21]. To our knowledge, the current research is the first study to divulge the strong *in vivo* efficacy of AsA against glioblastoma multiforme (GBM), the most aggressive form of glioma, as well as identifies underlying molecular mechanisms.

Apoptosis is a complex process involving several molecular events and signaling molecules [22–24]. Besides mitochondria, the central player in programmed cell death, other organelles such as endoplasmic reticulum (ER) and golgi bodies are actively involved in sensing stress stimuli and activating the cell suicide program [25–27]. Presently, there is abundant evidence for a direct and/or indirect ER role in apoptosis [26,28–30]. For example, stress signals culminating at the ER trigger rapid calcium release, activate calcium-dependent kinases and/or proteases involved in apoptosis [27–29]. In this regard, Bcl2 has been implicated in preventing the calcium release, while Bax induces calcium mobilization from ER calcium stores [27–29,31]. Besides activating the mitochondrial pathway, sustained ER stress can lead directly to apoptotic death by activating CHOP (CCAAT-enhancer-binding protein homologous protein), caspase 12/7, and Calpain [28,29]. In the present study, we examined the effect of AsA on apoptosis induction in GBM cells with a focus on pathways emanating from mitochondria and ER.

MATERIALS AND METHODS

Cell culture and reagents

GBM cells (LN18, U87MG, and U118MG) were procured from ATCC (Manassas, VA). LN18 cells were cultured in DMEM supplemented with 5% FBS, U87MG cells in Eagle's MEM supplemented with 10% FBS, and U118MG cells in DMEM supplemented with 10% FBS. U87MG-LUC cells were constructed by transducing U87MG cells with MSCV

Luciferase PGK, and clones were selected with hygromycin. AsA, rutin hydrate, MTT reagent, temozolomide (TMZ), crystal violet, haematoxylin and eosin were from Sigma-Aldrich (St. Louis, MO). Trypan blue was from Invitrogen (Carlsbad, CA). Antibodies for cleaved PARP, cleaved caspases (3, 9, and 8), Bid, Bad, GRP78, IRE1α, Calnexin, PDI, and Calpain were from Cell signaling (Danvers, MA). Survivin antibody was from Novus (Littleton, CO). α-Tubulin antibody was from Neomarkers (Fremont, CA). ECL detection system and anti-mouse HRP conjugated secondary antibody were from GE Healthcare (Buckinghamshire, UK). Protein assay kit was from Bio-Rad Laboratories (Hercules, CA). BAPTA and Fluo-3/AM were from Calbiochem (San Diego, CA). All other reagents were acquired in their highest purity grade available commercially.

Cell viability and clonogenic assays

Cell viability was measured by MTT assay as previously described [21]. For the clonogenic assay, GBM cells (1×10^3 cells per well) were seeded in six-well plates. Every 48 h, fresh media was added with DMSO or AsA (10–100 μM). On the 11^{th} day, cells were fixed in methanol and acetic acid mixture (3:1) for 10 min and stained with crystal violet dye (30 min).

Apoptosis assay and JC1 staining

Annexin V/PI staining was performed using Vybrant Apoptosis Assay Kit (Invitrogen, Eugene, OR) following vendor's protocol and flow cytometry was performed to quantitate apoptotic population. For JC1 (5,5′,6,6′-tetrachloro-1,1′,3,3′-tetraethylbenzimidazolyl-carbocyanine iodide) staining, at the end of AsA treatment, cells were incubated with JC1 dye (10 μg/ml; 10 min) and analyzed by flow cytometry.

Electron microscopy

LN18 cells were grown on permanox dishes, treated with AsA, and fixed with 2% paraformaldehyde/2% glutaraldehyde. Cells were post-fixed with 2% osmium tetroxide, infiltrated with epon/araldite epoxy resin, sectioned at 50–70 nm, and mounted on 200 mesh copper grids. Grids were post-stained with lead citrate and uranly acetate to enhance contrast. Sections were photographed using FEI Technai Transmission electron microscope equipped with Gatan Ultrascan digital high-resolution camera.

Western blotting

Whole-cell extracts were prepared and Western blotting was performed as previously described [21,32]. Autoradiograms/bands were scanned using Adobe Photoshop 6.0 (Adobe Systems, San Jose, CA, USA).

Calcium measurement

Free intracellular calcium was measured by fluorescent Fluo-3/AM following a previously reported protocol [14]. Briefly, GBM cells (50×10^3 cells per well) were seeded and treated with mentioned AsA dose (70–90 μM) and time-point (30 min to 12 h). At the end, media was removed and Fluo-3/AM (5.0 μM) was added. Thereafter, cells were harvested and

suspended in PBS containing PI (5.0 μg/ml). Signal from Fluo-3/AM bound to calcium was recorded by flow cytometry.

Xenograft study and Immunohistochemistry (IHC)

Athymic (*nu/nu*) male nude mice were housed at the University of Colorado Denver (UCD) animal care facility. Protocols were approved by UCD Institutional Animal Care and Use Committee. In the first AsA treatment protocol, ~1.0 million U87MG cells were suspended in matrigel and s.c. injected in each mouse (~ 8 weeks old) flanks. Next day, mice were randomly divided into two groups (n = 5 per group): Group I was treated with of 0.9% saline (200 μl) containing 0.01% tween 20 (vehicle control) and Group II was treated with AsA (30 mg/kg; 200 μl in 0.9% saline containing 0.01% tween 20). Treatments were dosed via oral gavage 7 days/week. Xenograft sizes were measured weekly in two dimensions using a digital caliper. The tumor volume was calculated by the formula: $0.5236\ L_1(L_2)^2$, where L_1 is the long diameter, and L_2 is the short diameter. At the end of the 4^{th} week, mice were euthanized, tumors were carefully dissected, weighed, and processed for IHC following published methods [33–35]. All the microscopic IHC analyses were performed using a Zeiss Axioscope 2 microscope (Carl Zeiss Inc., Jena, Germany) and photographs were captured (at 400X) with a Carl Zeiss AxioCam MrC5 camera with Axiovision Rel 4.5 software. In the second protocol, U87MG xenografts were initiated, and after 2 weeks of xenograft growth (~200 to 300 mm^3 tumor volume), mice were treated with vehicle or AsA as detailed above.

Orthotopic xenograft study and Animal imaging

Male athymic nude mice were anesthetized with isoflurane and immobilized in a stereotaxic apparatus (David Kopf Instruments, Tujunga, CA). U87MG-LUC cells (3×10^5 in 6 μl serum free medium) were injected at a rate of 500 nl/min at 2.5 mm lateral, 1.5 mm anterior and 3.5 mm ventral relative to bregma using a microUltra Pump (World Precision Instruments, IncSarasota, FL) and a Hamilton syringe. The incision was closed with Ethicon 5-0 vicryl sutures. Thereafter, mice were treated with either vehicle control (n = 5) or AsA (30 mg/kg/ twice a day, n = 5) as described above. After one month, orthotopic tumor growth was confirmed by bioluminescence imaging. Briefly, mice were intraperitoneally injected with 100 μL of 30 mg/mL D-luciferin and imaged using Xenogen IVIS200 imaging system. Thereafter, magnetic resonance imaging (MRI) was performed for volumetric assessment of tumor growth. Briefly, animals were injected intravenously with 0.2 mmol/kg of gadobenate dimeglumine (Multihance, Bracco Diagnostics, Princeton, NJ) via tail vein immediately prior to MRI. Animals were anesthetized with isoflurane (4% for induction, and 2–2.5% for MRI scans), placed into a custom-designed animal holder and inserted into a Bruker 4.7 Tesla MRI scanner (Bruker Medical, Billerica, MA). All MRI acquisitions were obtained using a bird-cage volumetric mouse body coil (36 mm diameter) which served as a transmitter/ receiver coil (tuned to proton resonance frequency at 200 MHz). After obtaining a tri-pilot localizer scan, Bruker spin-echo T1-weighted scans (MSME T1, Repetition time/ Echo time [TR/TE]=700/11 msec) were acquired followed by fast spin echo T2-weighted scans (RARE T2, TR/TE=4000/80 msec). The field of view was 3 cm, with slice sickness of 1 mm, containing 16 consequent axial slices which covered the entire brain region. For the analysis, gadolinium-enhanced T1- and hyperintense T2-areas were used. The calculation of tumor volumes was performed by manually placing region of interests (ROI) over the

hyperintense areas throughout each T1- and T2-MRI series. All post-processing analysis was performed using Bruker ParaVision v3.2.0 software.

LC/MS-MS analysis of AsA in mouse plasma and brain

An Applied Biosystems Sciex 4000 (Applied Biosystems; Foster City, CA) equipped with a Shimadzu HPLC (Shimadzu Scientific Instruments, Inc.; Columbia, MD) and Leap auto-sampler (LEAP Technologies; Carrboro, NC) was used. Liquid chromatography employed an Agilent Technologies Zorbax extended-C18 50 × 4.6 mm 5 micron column and column guard at 40 °C with a flow-rate of 0.4 mL/min. The mobile phase consisted of A: 10 mM (NH_4OAc), 0.1% formic acid in H_2O, and B: 50:50 ACN:MeOH (acetonitrile:methanol). The chromatography method used was 95% A for 1.0 min; ramped to 95% B at 6.0 min and held for 3.5 min, lastly, brought back to 95% A at 10.5 min and held for 1.5 min (12.0 min total run time). Compounds were monitored via electro-spray ionization negative ion mode (ESI −) using the following conditions: i) an ion-spray voltage of −4200 V; ii) temperature, 200 °C; iii) curtain gas (CUR; set at 35) and Collisionally Activated Dissociation (CAD; set at 12) gas were nitrogen; iv) Ion Source gas one (GS1) and two (GS2) were set to 40; v) entrance potential was set at 10 V; vi) quadruple one (Q1) and (Q3) were set on Low resolution; vii) dwell time was set at 200 msec; and viii) declustering potential (DP), collision energy (CE), and collision cell exit potential (CXP) are voltages (V) and were set to −10, −52, and −19, respectively. Samples (10 μL) were analyzed by LC/MS-MS. Rutin (IS; t_R = 4.6 min) LC/MS-MS: 609.1 → 299.8 *m/z*; Asiatic acid (t_R = 7.3 min) LC/MS-MS: 533.3 → 487.0 *m/z*. AsA displayed significantly higher sensitivity via electrospray negative ion mode (ESI −) compared to positive ion mode (ESI +). AsA was not prone to formation of daughter ions (Supplementary Figure 1); however, AsA had a significant propensity to form the formic acid complex when mixed with the extraction solution (Supplementary Figure 2). The complex appeared to be retained even during RP (reverse-phase) chromatography and provided us with a sensitive LC/MS-MS method to monitor AsA (Supplementary Figure 3) from biological samples.

Standard curves (SC) were prepared by addition and thorough mixing of various aqueous solutions (25 μL) into control plasma (425 μL). SC samples were mixed and immediately frozen (−80 ± 10 °C). An extraction solution containing rutin (0.25 μM) as the internal standard (IS) was freshly prepared in a 100 mL volumetric flask containing 4:1 (1:1 ACN:MeOH) and H_2O (v/v). The frozen SC and plasma samples were removed from the freezer and allowed to thaw on ice (20–30 min). The tubes were vortex mixed (3–5 sec), samples transferred into Eppendorf tubes and followed by addition of two volumes of extraction solution, capped, and mixed. After five min, vortex mixed an additional time (5 sec), and centrifuged at 10,000 rpm (10 min) using an Eppendorf minispin centrifuge (Hamburg, Germany). The supernatants were transferred into individual wells of a 96-well plate. The 96-well plate was placed into the LEAP auto-sampler cool-stack (7 ± 1 °C) and immediately analyzed via LC/MS-MS. A linear standard curve was observed (1 – 500 ng/ml) and the data was fitted to a $1/x^2$ weighted linear regression, R^2 = 0.9983. In the case of brain tissue, tissue was homogenized with two volumes of PBS (pH 7.4) and samples extracted and analyzed as detailed above.

Statistical analysis

Statistical analyses were performed with Sigma Stat software version 2.03 (Jandel scientific, San Rafael, CA). One-way ANOVA followed by Tukey's test was used for multiple comparisons and statistically significant difference was considered at $p \leq 0.05$.

RESULTS

AsA inhibits GBM cells survival with efficacy better than temozolomide (TMZ)

AsA (10–100 μM) treatment strongly inhibited human GBM LN18, U87MG and U118MG cell viability 6–24 h after treatment (Figure 1A). Importantly, at equimolar dose TMZ, a cytotoxic alkylating agent used clinically to treat gliomas [2,36], was not found to be effective against all three GBM cell lines (Figure 1B), suggesting that AsA efficacy against GBM may be better than TMZ. However, TMZ could be effective against GBM cells when treated for longer duration [37,38]. Next, we examined the long term effects of AsA exposure on GBM cells growth. GBM cells were plated at a low density (1000 cells per well), and every 48 h, fresh media was added with DMSO or AsA (10–100 μM). As depicted in Figure 1C, repetitive AsA exposure displayed an effective inhibition against GBM cell growth.

AsA inhibits U87MG xenograft growth

Based upon the strong efficacy observed with AsA against GBM cells in cell culture, we examined its *in vivo* efficacy. We employed the U87MG ectopic xenograft model and followed two AsA treatment protocols. In the first protocol, AsA (30 mg/kg/day) was orally administered starting one day after U87MG cell implantation. AsA administration for 4 weeks significantly decreased tumor volume and weight (Figure 2A-upper panels), but did not influence mice body weight or diet consumption (Figure 2A-bottom panels). In the second protocol, AsA (30 mg/kg/day) was administered two weeks after U87MG cell implantation. Here too, AsA caused significant decrease in U87MG xenograft volume and weight, even though mice in AsA group displayed slightly higher initial tumor volume (on administration day 0) (Figure 2B).

Next, plasma and brain tissue samples were analyzed by LC/MS-MS to detect AsA. In the first treatment protocol, immediately after the last AsA dose, we detected AsA plasma levels of 50.0 ± 11.8 ng/ml (mean ± SD) and brain tissue AsA levels of 4.7 ± 1.3 ng/g. In the second treatment protocol, plasma AsA levels were observed at 93.4 ng/ml, 258.7 ng/ml, 67.7 ng/ml and 63.8 ng/ml after 30 min, 1 h, 2 h and 4 h post last AsA dose; brain AsA levels were 4.2 ng/g, 5.2 ng/g, 2.7 ng/g and 2.8 ng/g, respectively.

IHC analysis of U87MG xenografts/tumors (from first treatment protocol) showed that AsA inhibited the immunostaining for cell proliferation biomarkers PCNA and Ki-67 (Figure 2C). AsA also increased the apoptotic death in U87MG tumors as evidenced by TUNEL and cleaved-caspase 3 (CC3) positive cells (Figure 2D). Importantly, AsA feeding did not affect the TUNEL-positive population in normal lung, liver and kidney tissues (Figure 2E).

AsA inhibits orthotopic U87MG xenograft growth

Next, we assessed AsA efficacy against U87MG xenograft growth in the brain microenvironment. We injected U87MG-LUC cells into the brain of nude mice. After 1 month, the growth of U87MG-LUC tumors in the brain was confirmed by bioluminescence in 9/10 mice (data not shown). Two weeks later, we measured the tumor volume by MRI, and at this time 10/10 mice illustrated tumor growth. As shown in Figure 3A and 3B, AsA feeding decreased the tumor volume by 60% compared to control group of mice, however this was not statistically significant. The tumor volumes in the AsA-treated group were in the range of 2.22 to 6.22 mm^3, while in untreated controls 1.92 to 23.2 mm^3. Tumor lesions were visible in 0–2 anatomical slices in the AsA-treated group (none mouse no tumor; 3 mice with 1 slice location; 2 mice with 2 slice tumor detection); while in the control group, 2–4 anatomical slices revealed large tumor volumes (3 mice with 2 slices, 1 mouse with 3 slices, and 1 mouse with 4 slices involvement). Overall, MRI data showed that AsA administration inhibited the growth of U87MG tumors in mouse brain.

AsA activates apoptotic machinery in GBM cells

To establish the nature of cell death caused by AsA in GBM cells, we next examined AsA effect on apoptosis. Annexin/PI staining data showed that AsA significantly increased the apoptotic population in LN18, U87MG, and U118MG cells (Figure 4A). Furthermore, JC1 staining results showed that AsA caused the loss of mitochondrial membrane potential in LN18, U87MG, and U118MG cells (Figure 4B) indicating apoptosis induction in these cells.

Next, we examined AsA effects on several molecular regulators of apoptosis. As shown in Figure 4C, AsA induced PARP cleavage and activated caspases (8, 9 and 3) in GBM cells but decreased Bid and Bcl2 expression. Furthermore, AsA decreased survivin expression in LN18 and U118MG, but not in U87MG cells (Figure 4C). A strong increase in Bad expression was observed in GBM cells with AsA treatment; however in LN18 cells, a slight decrease in Bad expression was noticeable with the highest AsA (70 μM) dose (Figure 4C). We also examined the role of caspase activation in AsA-mediated apoptosis; and in the presence of pan-caspase inhibitor (ZVAD-fmk), AsA-induced apoptosis was completely reversed in LN18 cells (Figure 4D). Similarly, ZVAD-fmk inhibited the AsA-induced PARP cleavage and caspases (8, 9, and 3) activation (Figure 4E). However, we did not observe any reversal of apoptosis in U87MG cells, and only a slight reversal was observed in U118MG cells in the presence of ZVAD-fmk (data not shown).

AsA increases free intracellular calcium in GBM cells

The increase in free intracellular calcium could induce rapid cell death [16,25,29]. To understand whether calcium signaling was involved in cell death induced by AsA, GBM cells were treated with AsA at a dose eliciting maximum apoptosis (Figure 4A) and subjected to Fluo-3/AM staining. We found that AsA increases free intracellular calcium levels in a time-dependent manner, and maximum increase was observed at 2, 4 and 12 h in LN18, U87MG and U118MG, respectively (Figure 5A). Next, we examined AsA effect on cell viability in the presence of a cytoplasmic calcium chelator (BAPTA). In LN18 cells, live cell numbers noticeably increased at 6 h when treated with AsA in the presence of BAPTA. Similarly, BAPTA presence significantly attenuated the AsA-induced cell death in

LN18 cells (Figure 5B). However, neither cell growth inhibition nor cell death induction by AsA was completely reversed by BAPTA suggesting only a partial dependence of AsA anti-proliferative effects on calcium. Similarly, AsA effects on cell viability and death were not significantly dependent or only partly dependent upon intracellular calcium levels in U87MG and U118MG cells (Figure 5C and 5D).

AsA induces ER stress in GBM cells

ER is the calcium reservoir of the cells and an increase in intracellular calcium by AsA suggests that it causes ER stress. Accordingly, we examined AsA effects on the molecules related to ER stress (Figure 6A and 6B). As shown in Figure 6A in GBM cells, AsA increased the GRP78 level – an indicator of ER stress [29], and decreased the Calnexin level, a chaperone involved in protein folding [29]. Confocal microscopy results confirmed that AsA treatment increased GRP78 (FITC-green) and decreased Calnexin (FITC-green) expression in LN18 cells (Figure 6B). However, AsA did not affect the PDI (protein-disulphide isomerase), which is involved in stabilizing protein folding by catalyzing the formation of disulfide bonds (Figure 6A). Further, AsA treatment decreased the expression of IRE1α (Figure 6A), an ER-trans-membrane glycoprotein that is activated in response to unfolded protein response [29]. Importantly, AsA increased Calpain expression, a calcium-dependent protease which, when activated, plays a role in caspase activation and cellular dismantling [25,29,39]. Along with molecular alterations associated with ER stress, electron microscopy results illustrated that AsA affected the cytoskeletal organization of LN18 cells (Figure 6C). AsA treatment caused nuclear condensation, separation of cytoplasmic content from nuclei, and elongated ER structures (Figure 6C). Furthermore, IHC analyses of U87MG ectopic xenograft tissues showed that AsA significantly enhanced the level of GRP78 and Calpain (Figure 6D).

DISCUSSION

Malignant gliomas have the capacity to proliferate uncontrollably, sustain excessive angiogenesis, invade aggressively, and infiltrate different areas of the brain [40–42]. Over the past few decades, there has been little to no improvement in glioma patient survival [40,42]. Temozolomide is an FDA approved drug which is most commonly employed in clinic either alone or in combination with radiotherapy to treat GBM. However, within a few months of treatment, GBM cells develop resistance and relapse. Therefore, there is an urgent need for additional preventive and therapeutic drugs against GBM. Our current results illustrate that AsA, a natural non-toxic triterpene, is highly efficacious against GBM.

AsA is the active constituent present in *Centella asiatica*, an herb popularly known as Gotu kola in Chinese, Indian Pennywort in English, Brahmi in Hindi and Manduukaparani in Ayurveda [43]. In traditional medicine system, this herb and its constituents are held in high esteem for their efficacy in preventing brain aging and neuro-degeneration, regeneration of neural tissues, relieving stress and boosting memory [3,4,8,9,43,44]. In recent studies, AsA has shown tremendous anti-cancer efficacy [12–21], and considering its health benefits especially against neurological disorders [9–11], it is reasonably enticing to test this agent for the prevention and treatment of brain cancers. Earlier, we have reported in cell culture

models that AsA decreases VEGF secretion from GBM cells and inhibits their capability to promote angiogenesis in brain endothelial cells [21]. The current study further confirmed the broad spectrum efficacy of AsA against human GBM cells, and a few highlights from this study are: a) this is the first study showing the *in vivo* efficacy of AsA against human GBM cells without apparent toxicity; b) AsA is orally bioavailable as it was detected in plasma and brain tissue; c) AsA possesses higher efficacy against GBM cells compared to the FDA approved drug temozolomide under our treatment conditions; and d) AsA targets multiple signaling pathways inducing ER stress and apoptotic death in GBM cells.

Our findings also identified the molecular targets of AsA *in vivo* in terms of an increase in GRP78, Calpain and cleaved caspase 3 in U87MG tumors. Together, these *in vitro* and *in vivo* results as well as earlier published studies [14,16,19] suggest that AsA-mediated ER stress and enhanced intracellular calcium may be important for inducing programmed cell death in cancer cells. It is important to note that AsA activated the GRP78, confirming ER stress; however, it reduced the IRE1α and Calnexin expression in GBM cells. These results suggest that AsA induces ER stress in GBM cells but inhibits pathway/s that could ameliorate stress; and the excessive ER stress accompanied with calcium release and enhanced Calpain level activates apoptotic machinery. Furthermore, we observed a decrease in Bcl2 expression in GBM cells with AsA treatment. Even though the present study has not identified the sub-cellular localization of Bcl2, we speculate that AsA-mediated increase in intracellular calcium is partially through inhibiting Bcl2 expression in the ER. Another interesting aspect of the present study is that we observed strong biological anticancer efficacy of AsA in all three GBM cell lines but mechanistic studies revealed differences in the mechanism of AsA action depending upon the cell type. For example, AsA-induced apoptotic death was caspase-dependent in LN18 cells but was caspase-independent in U87MG and U118MG cells. Similarly, there were cell line based differences in the intracellular calcium role in AsA-mediated cell growth inhibition and cell death induction in GBM cells. More studies are warranted to substantiate these differential AsA mechanisms but these could be due to the dissimilarities in the origin, molecular and genetic differences among GBM cell lines.

One of the major constraints in treating GBM is the blood-brain barrier (BBB) that largely restricts the potential benefits of chemotherapeutic drugs. There have been numerous studies supporting the neuroprotective role of AsA but to our knowledge there is no reported data confirming its bioavailability into the brain tissues. Though earlier studies have identified plasma bioavailability of AsA in beagle dog and humans [45,46], the present results include the first report showing that orally administered AsA crosses the BBB in mice. Further studies are needed to identify the mechanism/s through which AsA crosses the BBB as well as the levels and biological activity of potential AsA metabolic products (AsA glucuronide and sulphate).

Overall, the present study is significant as we identified that orally bioavailable AsA could effectively target GBM cells both *in vitro* and *in vivo*. Importantly, the anticancer efficacy of AsA reported here could be translated in patients without toxicity, as based upon Hoh et al criterion[47], AsA dose used in the orthotopic xenograft study (30 mg/kg/twice daily) extrapolates to 180 mg AsA per person twice daily, assuming a body surface area of 1.8 m^2

accompanying a body weight of 70 kg. AsA is currently marketed as a supplement for several health benefits with a recommended 150–750 mg/daily dose of standardized extract of *Centella asiatica*. Based upon these extrapolations, it is tempting to propose AsA role in the prevention of GBM. In the future, we also need to test whether the anti-GBM efficacy of AsA could be further enhanced by dose escalation, other modes of administration (such as in diet) or through better formulation. Also, we need to establish AsA efficacy in patient-derived xenograft model before testing it in patients.

In conclusion, results from the present study illustrate that AsA induces apoptotic death in GBM cells through activating caspases and modulating the expression of Bcl2 family members and survivin. Furthermore, AsA affected the expression of several signaling molecules causing ER stress and enhanced the free intracellular calcium in GBM cells. Together, these molecular alterations contribute to the strong efficacy of AsA against GBM cells. Considering AsA non-toxicity, long history of successful use in traditional medicinal system and beneficial health effects in humans, results from the present study advocate further pre-clinical and clinical evaluation of AsA against gliomas.

Supplementary Material

Refer to Web version on PubMed Central for supplementary material.

Acknowledgments

Grant Support: This work was supported by Department of Pharmaceutical Sciences (DOPS) Seed Grant (to GD) and NCI RO1 grant CA102514 (to RA).

The research utilized services of Medicinal Chemistry Core facility (MFW) partly funded via CCTSI grant 5UL1RR025780 from NCRR/NIH. FACS and imaging shared resources supported by CCSG P30CA046934 were utilized.

List of Abbreviations

ANOVA	Analysis of variance
AsA	Asiatic acid
BBB	Blood-brain barrier
CHOP	CCAAT-enhancer-binding protein homologous protein
DP	Declustering potential
ER	Endoplasmic reticulum
GBM	Glioblastoma multiforme
GRP78	Glucose regulated protein 78
IHC	Immunohistochemistry
IRE1α	Inositol-requiring enzyme 1 alpha
LC/MS	Liquid chromatography-mass spectrometry
MRI	Magnetic resonance imaging

MTT	3-(4,5-dimethylthiazol-2-yl)-2,5-diphenyltetrazolium bromide
PARP	Poly ADP ribose polymerase
PCNA	Proliferating cell nuclear antigen
PDI	Protein disulfide isomerase
PI	Propidium iodide
TMZ	Temozolomide
TUNEL	Terminal deoxynucleotidyl transferase d UTP nick end labeling

References

1. Fan S, Sun Z, Jiang D, et al. BmKCT toxin inhibits glioma proliferation and tumor metastasis. Cancer Lett. 2010; 291:158–166. [PubMed: 19906483]
2. Friedman HS, Kerby T, Calvert H. Temozolomide and treatment of malignant glioma. Clin Cancer Res. 2000; 6:2585–2597. [PubMed: 10914698]
3. Brinkhaus B, Lindner M, Schuppan D, Hahn EG. Chemical, pharmacological and clinical profile of the East Asian medical plant Centella asiatica. Phytomedicine. 2000; 7:427–448. [PubMed: 11081995]
4. James JT, Dubery IA. Pentacyclic triterpenoids from the medicinal herb, Centella asiatica (L.). Urban Molecules. 2009; 14:3922–3941.
5. Shinomol GK, Muralidhara. Prophylactic neuroprotective property of Centella asiatica against 3-nitropropionic acid induced oxidative stress and mitochondrial dysfunctions in brain regions of prepubertal mice. Neurotoxicology. 2008; 29:948–957. [PubMed: 18930762]
6. Soumyanath A, Zhong YP, Henson E, et al. Centella asiatica Extract Improves Behavioral Deficits in a Mouse Model of Alzheimer's Disease: Investigation of a Possible Mechanism of Action. Int J Alzheimers Dis. 2012; 2012:381974. [PubMed: 22506133]
7. Soumyanath A, Zhong YP, Gold SA, et al. Centella asiatica accelerates nerve regeneration upon oral administration and contains multiple active fractions increasing neurite elongation in-vitro. J Pharm Pharmacol. 2005; 57:1221–1229. [PubMed: 16105244]
8. Singh RH, Narsimhamurthy K, Singh G. Neuronutrient impact of Ayurvedic Rasayana therapy in brain aging. Biogerontology. 2008; 9:369–374. [PubMed: 18931935]
9. Krishnamurthy RG, Senut MC, Zemke D, et al. Asiatic acid, a pentacyclic triterpene from Centella asiatica, is neuroprotective in a mouse model of focal cerebral ischemia. J Neurosci Res. 2009; 87:2541–2550. [PubMed: 19382233]
10. Lee MK, Kim SR, Sung SH, et al. Asiatic acid derivatives protect cultured cortical neurons from glutamate-induced excitotoxicity. Res Commun Mol Pathol Pharmacol. 2000; 108:75–86. [PubMed: 11758977]
11. Xu MF, Xiong YY, Liu JK, Qian JJ, Zhu L, Gao J. Asiatic acid, a pentacyclic triterpene in Centella asiatica, attenuates glutamate-induced cognitive deficits in mice and apoptosis in SH-SY5Y cells. Acta Pharmacol Sin. 2012; 33:578–587. [PubMed: 22447225]
12. Tang XL, Yang XY, Jung HJ, et al. Asiatic acid induces colon cancer cell growth inhibition and apoptosis through mitochondrial death cascade. Biol Pharm Bull. 2009; 32:1399–1405. [PubMed: 19652380]
13. Hsu YL, Kuo PL, Lin LT, Lin CC. Asiatic acid, a triterpene, induces apoptosis and cell cycle arrest through activation of extracellular signal-regulated kinase and p38 mitogen-activated protein kinase pathways in human breast cancer cells. J Pharmacol Exp Ther. 2005; 313:333–344. [PubMed: 15626723]
14. Cho CW, Choi DS, Cardone MH, Kim CW, Sinskey AJ, Rha C. Glioblastoma cell death induced by asiatic acid. Cell Biol Toxicol. 2006; 22:393–408. [PubMed: 16897440]

15. Park BC, Bosire KO, Lee ES, Lee YS, Kim JA. Asiatic acid induces apoptosis in SK-MEL-2 human melanoma cells. Cancer Lett. 2005; 218:81–90. [PubMed: 15639343]
16. Gurfinkel DM, Chow S, Hurren R, et al. Disruption of the endoplasmic reticulum and increases in cytoplasmic calcium are early events in cell death induced by the natural triterpenoid Asiatic acid. Apoptosis. 2006; 11:1463–1471. [PubMed: 16820960]
17. Meng YQ, Li YY, Li FQ, et al. Synthesis and antitumor activity evaluation of new asiatic acid derivatives. J Asian Nat Prod Res. 2012; 14:844–855. [PubMed: 22924623]
18. Bunpo P, Kataoka K, Arimochi H, et al. Inhibitory effects of asiatic acid and CPT-11 on growth of HT-29 cells. J Med Invest. 2005; 52:65–73. [PubMed: 15751275]
19. Lee YS, Jin DQ, Kwon EJ, et al. Asiatic acid, a triterpene, induces apoptosis through intracellular Ca2+ release and enhanced expression of p53 in HepG2 human hepatoma cells. Cancer Lett. 2002; 186:83–91. [PubMed: 12183079]
20. Park BC, Paek SH, Lee YS, et al. Inhibitory effects of asiatic acid on 7,12-dimethylbenz[a]anthracene and 12-O-tetradecanoylphorbol 13-acetate-induced tumor promotion in mice. Biol Pharm Bull. 2007; 30:176–179. [PubMed: 17202682]
21. Kavitha CV, Agarwal C, Agarwal R, Deep G. Asiatic Acid inhibits pro-angiogenic effects of VEGF and human gliomas in endothelial cell culture models. PLoS One. 2011; 6:e22745. [PubMed: 21826202]
22. Igney FH, Krammer PH. Death and anti-death: tumour resistance to apoptosis. Nat Rev Cancer. 2002; 2:277–288. [PubMed: 12001989]
23. Riedl SJ, Salvesen GS. The apoptosome: signalling platform of cell death. Nat Rev Mol Cell Biol. 2007; 8:405–413. [PubMed: 17377525]
24. Cotter TG. Apoptosis and cancer: the genesis of a research field. Nat Rev Cancer. 2009; 9:501–507. [PubMed: 19550425]
25. Wlodkowic D, Skommer J, McGuinness D, Hillier C, Darzynkiewicz Z. ER-Golgi network--a future target for anti-cancer therapy. Leuk Res. 2009; 33:1440–1447. [PubMed: 19595459]
26. Ferri KF, Kroemer G. Organelle-specific initiation of cell death pathways. Nat Cell Biol. 2001; 3:E255–263. [PubMed: 11715037]
27. Hoyer-Hansen M, Jaattela M. Connecting endoplasmic reticulum stress to autophagy by unfolded protein response and calcium. Cell Death Differ. 2007; 14:1576–1582. [PubMed: 17612585]
28. Schwarze SR, Lin EW, Christian PA, Gayheart DT, Kyprianou N. Intracellular death platform steps-in: targeting prostate tumors via endoplasmic reticulum (ER) apoptosis. Prostate. 2008; 68:1615–1623. [PubMed: 18663729]
29. Boelens J, Lust S, Offner F, Bracke ME, Vanhoecke BW. Review. The endoplasmic reticulum: a target for new anticancer drugs. In Vivo. 2007; 21:215–226. [PubMed: 17436569]
30. Kraskiewicz H, FitzGerald U. InterfERing with endoplasmic reticulum stress. Trends Pharmacol Sci. 2012; 33:53–63. [PubMed: 22112465]
31. Oakes SA, Opferman JT, Pozzan T, Korsmeyer SJ, Scorrano L. Regulation of endoplasmic reticulum Ca2+ dynamics by proapoptotic BCL-2 family members. Biochem Pharmacol. 2003; 66:1335–1340. [PubMed: 14555206]
32. Zi X, Feyes DK, Agarwal R. Anticarcinogenic effect of a flavonoid antioxidant, silymarin, in human breast cancer cells MDA-MB 468: induction of G1 arrest through an increase in Cip1/p21 concomitant with a decrease in kinase activity of cyclin-dependent kinases and associated cyclins. Clin Cancer Res. 1998; 4:1055–1064. [PubMed: 9563902]
33. Singh RP, Deep G, Chittezhath M, et al. Effect of silibinin on the growth and progression of primary lung tumors in mice. J Natl Cancer Inst. 2006; 98:846–855. [PubMed: 16788158]
34. Singh RP, Deep G, Blouin MJ, Pollak MN, Agarwal R. Silibinin suppresses in vivo growth of human prostate carcinoma PC-3 tumor xenograft. Carcinogenesis. 2007; 28:2567–2574. [PubMed: 17916909]
35. Gu M, Singh RP, Dhanalakshmi S, Agarwal C, Agarwal R. Silibinin inhibits inflammatory and angiogenic attributes in photocarcinogenesis in SKH-1 hairless mice. Cancer Res. 2007; 67:3483–3491. [PubMed: 17409458]
36. Wick W, Weller M, Weiler M, Batchelor T, Yung AW, Platten M. Pathway inhibition: emerging molecular targets for treating glioblastoma. Neuro Oncol. 2011; 13:566–579. [PubMed: 21636705]

37. Hirose Y, Berger MS, Pieper RO. p53 effects both the duration of G2/M arrest and the fate of temozolomide-treated human glioblastoma cells. Cancer Res. 2001; 61:1957–1963. [PubMed: 11280752]

38. Yamini B, Yu X, Gillespie GY, Kufe DW, Weichselbaum RR. Transcriptional targeting of adenovirally delivered tumor necrosis factor alpha by temozolomide in experimental glioblastoma. Cancer Res. 2004; 64:6381–6384. [PubMed: 15374943]

39. Guicciardi ME, Gores GJ. Calpains can do it alone: implications for cancer therapy. Cancer Biol Ther. 2003; 2:153–154. [PubMed: 12750553]

40. Lefranc F, Sadeghi N, Camby I, Metens T, Dewitte O, Kiss R. Present and potential future issues in glioblastoma treatment. Expert Rev Anticancer Ther. 2006; 6:719–732. [PubMed: 16759163]

41. Tate MC, Aghi MK. Biology of angiogenesis and invasion in glioma. Neurotherapeutics. 2009; 6:447–457. [PubMed: 19560735]

42. Lefranc F, Brotchi J, Kiss R. Possible future issues in the treatment of glioblastomas: special emphasis on cell migration and the resistance of migrating glioblastoma cells to apoptosis. J Clin Oncol. 2005; 23:2411–2422. [PubMed: 15800333]

43. Zheng CJ, Qin LP. Chemical components of Centella asiatica and their bioactivities. Zhong Xi Yi Jie He Xue Bao. 2007; 5:348–351. [PubMed: 17498500]

44. Dhanasekaran M, Holcomb LA, Hitt AR, et al. Centella asiatica extract selectively decreases amyloid beta levels in hippocampus of Alzheimer's disease animal model. Phytother Res. 2009; 23:14–19. [PubMed: 19048607]

45. Zheng XC, Wang SH. Determination of asiatic acid in beagle dog plasma after oral administration of Centella asiatica extract by precolumn derivatization RP-HPLC. J Chromatogr B Analyt Technol Biomed Life Sci. 2009; 877:477–481.

46. Grimaldi R, De Ponti F, D'Angelo L, et al. Pharmacokinetics of the total triterpenic fraction of Centella asiatica after single and multiple administrations to healthy volunteers. A new assay for asiatic acid. J Ethnopharmacol. 1990; 28:235–241. [PubMed: 2329813]

47. Hoh C, Boocock D, Marczylo T, et al. Pilot study of oral silibinin, a putative chemopreventive agent, in colorectal cancer patients: silibinin levels in plasma, colorectum, and liver and their pharmacodynamic consequences. Clin Cancer Res. 2006; 12:2944–2950. [PubMed: 16675592]

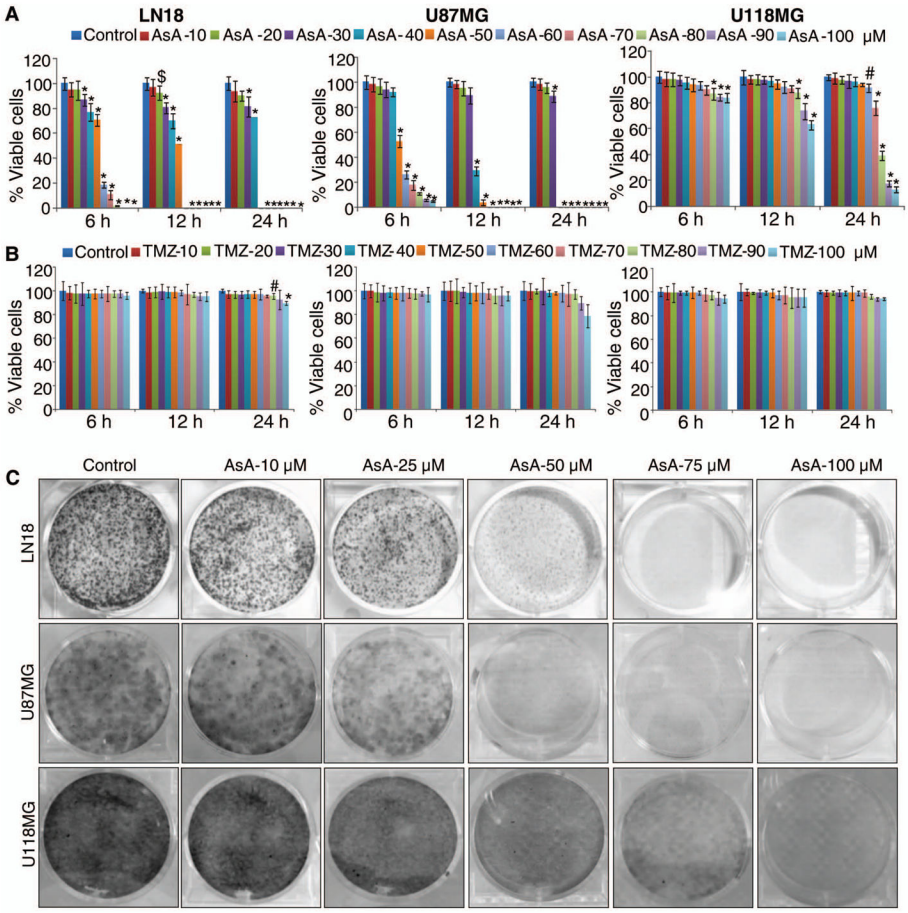

Figure 1.

AsA inhibits the survival of human GBM cells with efficacy better than temozolomide (TMZ). **(A–B)** GBM cells were treated with AsA or TMZ (10–100 μM) and MTT assay was performed at indicated time points. *, $p \leq 0.001$; #, $p \leq 0.01$; $, $p \leq 0.05$ **(C)** GBM cells were treated with AsA (10–100 μM) and clone formation was examined as described in methods.

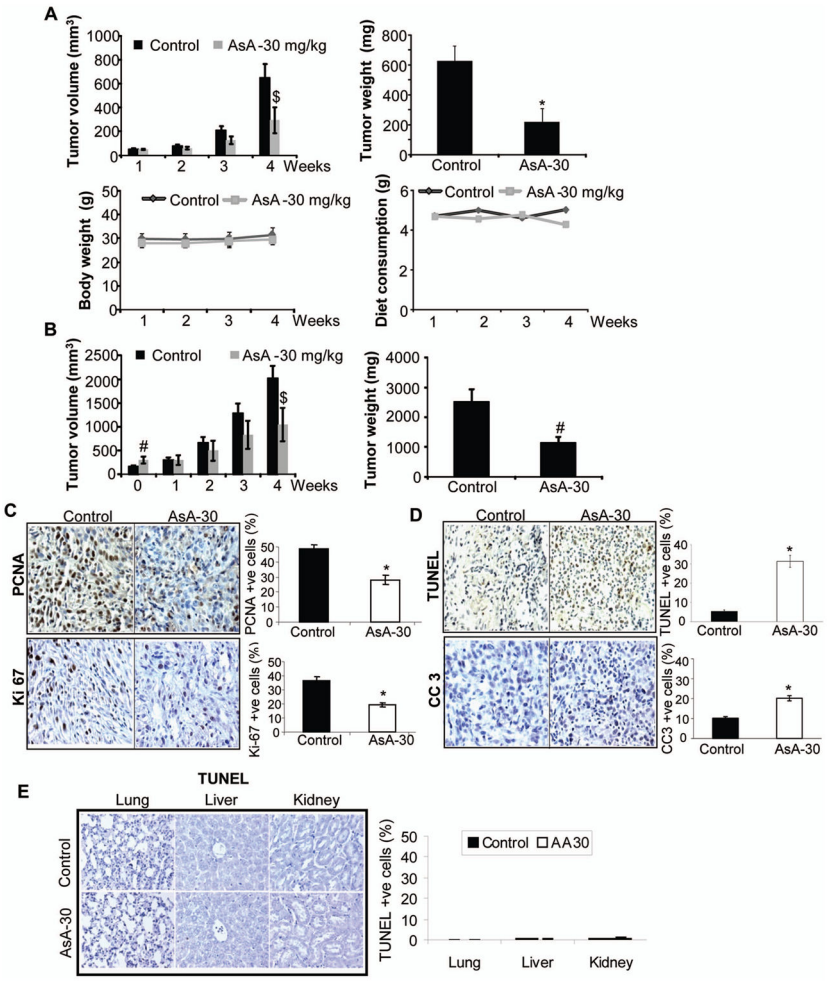

Figure 2.

In vivo efficacy of orally administered AsA against U87MG ectopic xenografts. **(A)** U87MG xenografts were initiated, and mice were gavaged either saline or AsA as detailed in methods. Data shown are: Tumor volume (in mm^3) as a function of time (upper left panel); tumor weight (mg) per mouse at the end of study (upper right panel); average body weight (g) per mouse as a function of time (lower left panel); and average diet weight consumption per mouse per day (lower right panel). **(B)** U87MG xenografts were initiated, and once xenografts achieved approximately 200 to 300 mm^3 tumor volume, mice were gavaged with saline or AsA. Data shown are: tumor volume (in mm^3) as a function of time (left panel) and tumor weight (g) per mouse at the end of study (right panel). **A** & **B** data are mean±SEM from 5 mice in each group with 10 xenografts. **(C–D)** U87MG xenografts were analyzed by IHC for proliferation biomarkers (PCNA and Ki-67) and apoptosis (TUNEL and CC3). Percentage of PCNA, Ki-67, TUNEL, and CC3 positive cells was calculated by counting the number of positive stained cells (brown stained) and the total number of cells at five arbitrarily selected fields from each tumor at 400x magnification. The data shown in the bar diagrams is the mean±SEM of 7–10 samples. **(E)** Lungs, liver and kidneys from each mouse (U87MG ectopic xenograft experiment) were analyzed for apoptosis by TUNEL. TUNEL-

positive cells are shown in the bar diagram as mean±SEM of 3–5 samples. *, $p \leq 0.001$; #, $p \leq 0.01$; $, $p \leq 0.05$

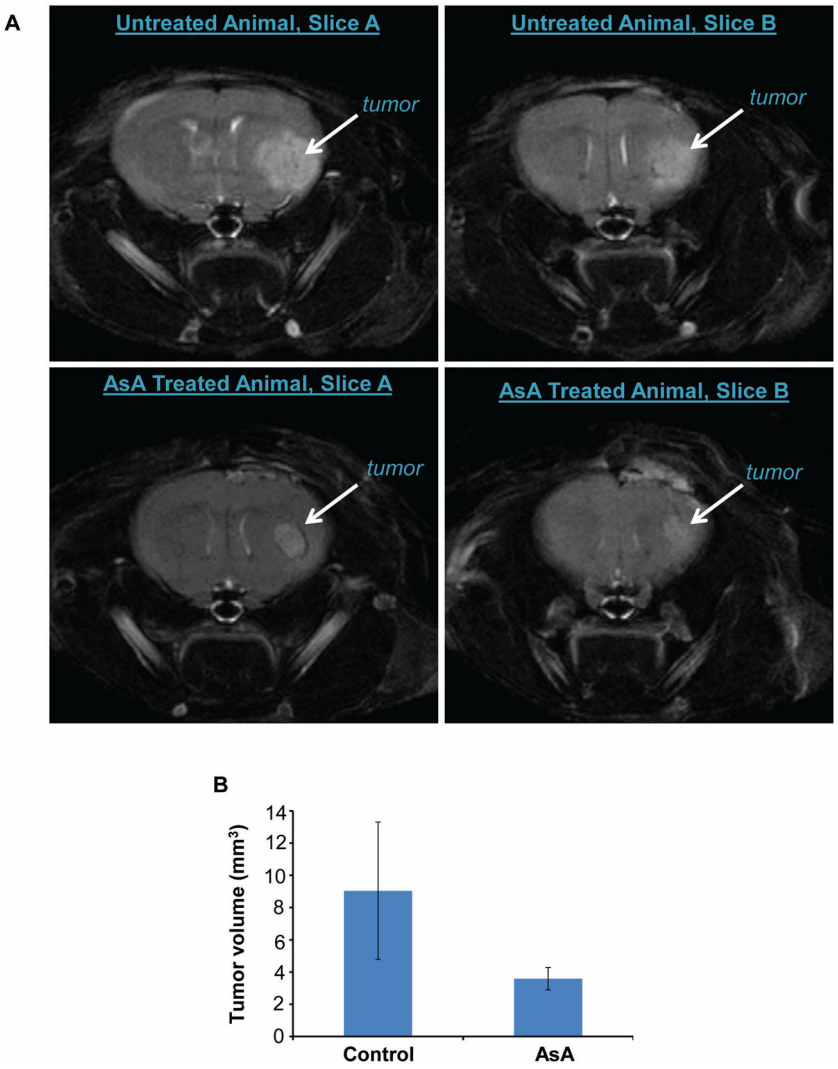

Figure 3.

Efficacy of orally administered AsA against U87MG orthotopic xenograft growth. **(A–B)** Volumetric assessment of the orthotopic tumors was done by MRI. Representative brain T_2-MRI images (two sequential MRI slices each from control and AsA-treated mice are shown) and average tumor volume (mean±SEM) are presented.

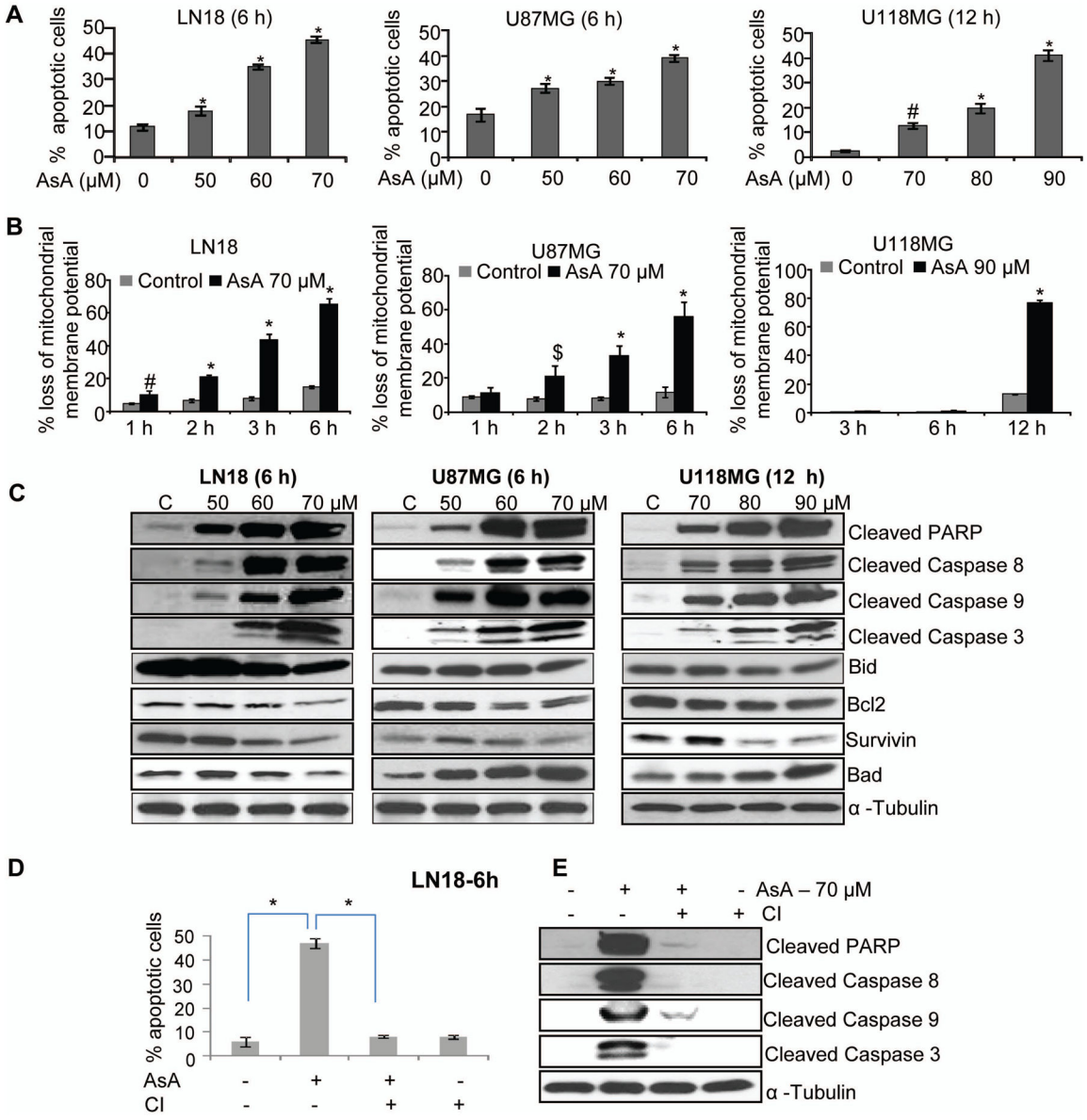

Figure 4.

AsA activates apoptotic machinery in human GBM cells. **(A–B)** AsA effect on apoptosis and mitochondrial membrane potential (MMP) in GBM cells was analyzed by annexin V/PI and JC1 staining, respectively. **(C)** GBM cells were treated with AsA for indicated duration and Western blotting was performed. **(D–E)** LN18 cells were pre-treated for 2 h with pan-caspase inhibitor (CI) Z-VAD.fmk (50 μM) and subsequently incubated with DMSO or AsA (70 μM) for additional 6 h. Thereafter, cells were analyzed for apoptosis by annexin V/PI staining. Under similar treatment conditions, total cell lysates were prepared and immunoblotted for the indicated proteins. Protein loading was monitored by re-probing the membrane with α-tubulin antibody. *, $p \leq 0.001$; #, $p \leq 0.01$; $, $p \leq 0.05$

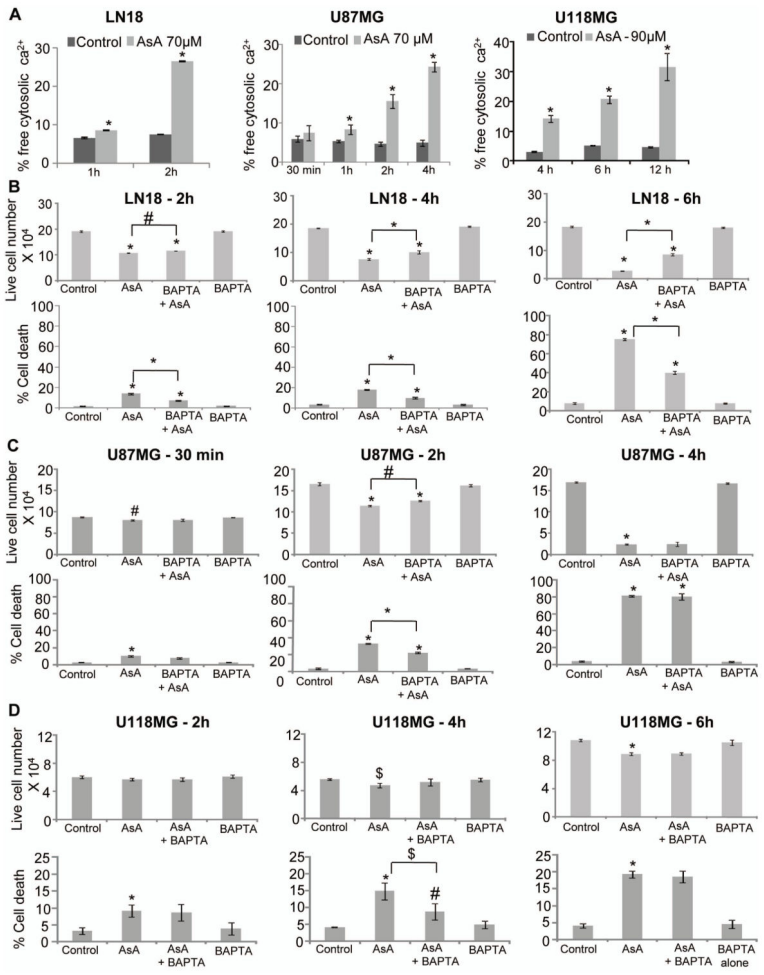

Figure 5.

Role of calcium in the anti-proliferative efficacy of AsA against GBM cells. **(A)** Effect of AsA treatment on free cytosolic calcium level in GBM cells was examined as described in methods. **(B, C & D)** GBM cells were pre-treated for 3 h with intracellular calcium chelator BAPTA (5 μM) followed by AsA treatment at indicated dose and time-point. At the end, both adherent and non-adherent cells were collected and live cell number and dead cell percentage were measured by trypan blue exclusion assay. *, $p \leq 0.001$; #, $p \leq 0.01$; $, $p \leq 0.05$

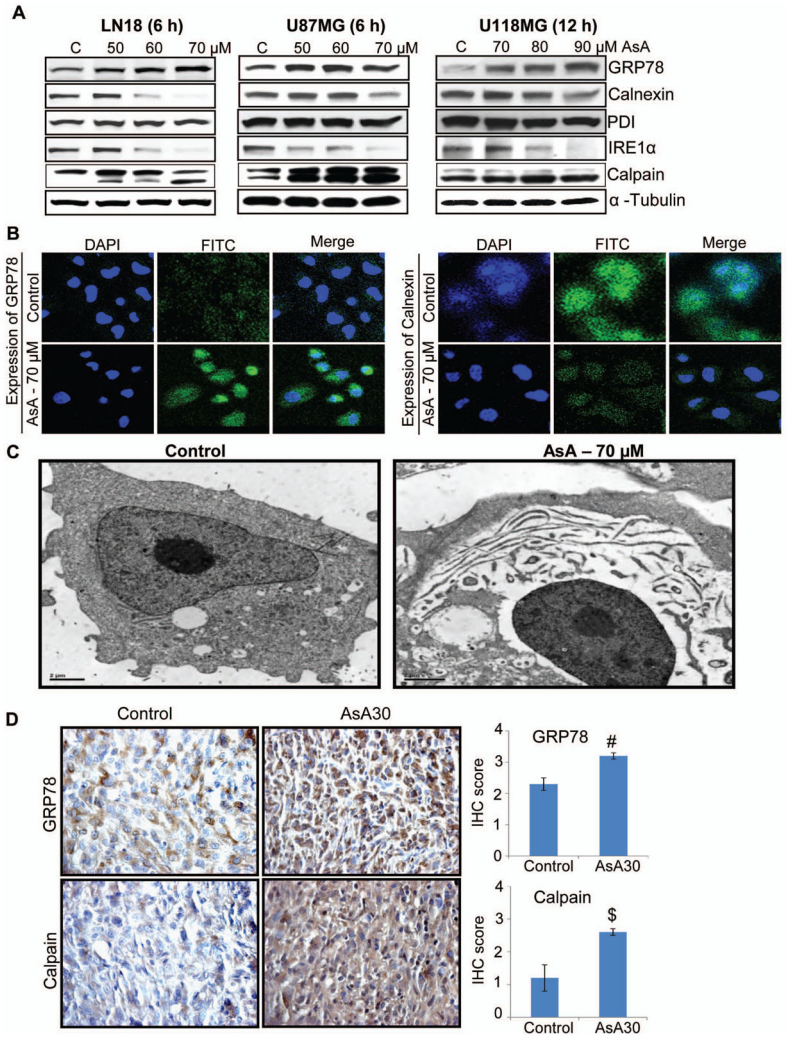

Figure 6.

AsA induces ER stress in GBM cells both *in vitro* and *in vivo*. **(A)** GBM cells were treated with AsA and the expression of ER stress markers was analyzed by Western blotting. Protein loading was monitored by re-probing the membrane with α-tubulin antibody. **(B)** LN18 cells were grown on cover slips and treated with 70 μM AsA for 6 h and processed for immunofluorescence for GRP78 (FITC-green) and Calnexin (FITC-green) expression. DAPI-blue was used to stain the nuclei. **(C)** LN18 cells were treated with 70 μM AsA for 2 h and analyzed by electron microscopy for AsA effect on cellular organization. **(D)** U87MG ectopic xenografts were analyzed for GRP78 and Calpain expression. Immunoreactivity of GRP78 and Calpain was analyzed in 5 random areas for each tumor tissue and was scored as 0+ (no staining), 1+ (weak staining), 2+ (moderate staining), 3+ (strong staining), 4+ (very strong staining). IHC scores (as mean±SEM) for GRP78 and Calpain in control versus AsA30 are shown as bar diagram of 5 samples. #, $p \leq 0.01$; $, $p \leq 0.05$